Proceedings of the Institution of Mechanical Engineers, Part G: Journal of Aerospace Engineering,
Volume 221, Number 5 (January 2007), pp. 679-690

Experimental observations of an 8 m/s drop test of a metallic helicopter underfloor structure onto water: part 2

K Hughes*, **R Vignjevic,** and **J Campbell**
Crashworthiness, Impacts and Structural Mechanics Group, School of Engineering (CISM), Cranfield University, Cranfield, Bedfordshire, UK

The manuscript was received on 30 March 2007 and was accepted after revision for publication on 10 July 2007.

DOI: 10.1243/09544100JAERO228

Abstract: This is the second part of a two-part paper that describes the experimental observations for two similar sections of floor that were dropped onto both hard and water surfaces at 8 m/s, as part of one experimental campaign. The current paper provides an assessment of a simple box-beam under floor structure typically found in metallic helicopters and provides an overview of the failure modes and the collapse mechanism observed when dropped onto water at 8 m/s, as well as providing quantitative data for the skin deflections observed.

The results demonstrate that the lack of frame and intersection joint collapse is a common feature, which is caused by the high failure strength of the existing construction, together with the inability of the skin to generate membrane loads that are sufficiently large to trigger progressive collapse within the structure. It is therefore recommended to reduce the collapse force of the structure through the use of geometry, material type, and inclusion of triggers. However, the caveat with this approach is that if the failure strength is optimized for a water impact, a poor crashworthy response may occur during a hard surface impact.

The current paper discusses three main limitations with the design, which are heavily interrelated, as improvements in frame and joint collapse cannot be achieved without considering developing the ductile behaviour of the skin. However, maintaining skin integrity will be critical to maintain the floatation capabilities of the helicopter. The current paper recommends that a next generation design should encompass a passive dual role capability for both hard and soft surface impacts, by being able to degrade the localized strength depending upon the type of surface encountered. This will significantly improve the crashworthy response of a metallic under floor structure and have a significant impact on improving occupant survivability for an impact on water.

Keywords: crashworthiness, helicopter, testing, water, failure, design

1 INTRODUCTION

The earliest recorded work that investigates the effects of a man-made object impacting on water can be traced back to 1929, where von Karman developed the first theoretical model to calculate the forces encountered during rigid seaplane floats impacting onto water [**1**]. This approach utilized the concept of added mass, which was a difficult parameter to quantify, but provided a good starting point for developing understanding in this field, which was subsequently extended and adopted during later works.

In the early days of helicopter crashworthiness development, a small cross-section of experimental data was available. Typically, these were reviewed by separate agencies and the information was generally fragmented, making it difficult to identify potential design improvements, or amend current regulations.

This problem was first addressed in 1986 by providing a historical review of civil helicopter accidents

**Corresponding author: Crashworthiness, Impact and Structural Mechanics Group (CISM), School of Engineering, Cranfield University, Building 52, Cranfield, Bedfordshire MK43 0AL, UK. email: k.hughes@cranfield.ac.uk*

occurring between 1974 and 1978, which was later followed by a review of US Navy and Army accidents in the same year [**2**, **3**]. This was again reviewed in 1993 for helicopter ditchings onto water that occurred between 1982 and 1989. This was performed in two phases, where part I dealt with the analysis of the impact and postimpact conditions [**4**], and part II provided an assessment of the structural response on occupant injury, the identification of ways of alleviating injury, together with an evaluation of current numerical techniques for modelling impacts onto water [**5**]. Several full-scale helicopter drop tests have also been performed in recent years in order to provide a greater understanding of the phenomena associated with fluid-structure interactions [**6–8**], as well as dedicated European research projects [**9**, **10**].

The design of the current fleet of helicopters has mainly concentrated upon impacts on hard surfaces, as this was deemed the most typical scenario encountered for their use. The energy of the impact is mainly absorbed through the progressive collapse of the frames and longerons in the underfloor, as well as through the stroke of the landing gear. This combined crushing reduces the decelerative loads experienced by the occupants, with the outer skin of the helicopter playing no part in the energy absorbing process.

This water environment poses a unique design case, for which conventional designs perform poorly, in terms of transmitting the water pressure and the absorption of energy. The existing crumple potential of the substructure is not utilized due to the lower loads encountered, where the mechanism for load transfer is dominated by the membrane response of the skin, which may fail as a result. This poor load transmission, coupled with a high failure strength of the surrounding structure, means that frame collapse does not occur and high forces and accelerations are passed through the airframe. This in turn can lead to the distortion of the passenger floor and preventing the energy absorbing seats from operating effectively, through to the jamming or loss of the doors. A more serious problem concerns loss in floatation capability if skin integrity fails and the resulting internal secondary damage that will ensue. Different solutions have been proposed in the past, namely sinewave beams [**11**, **12**] and tensor skin concepts [**13**], together with retrofit solutions [**14**].

This two part paper will complement existing research, by providing a summary of the experimental observations of a detailed European experimental campaign that involved assessing the crashworthiness of a conventional metallic under floor to both hard and water surfaces. The CAST project, which is an acronym for 'Crashworthiness of Helicopters on Water: Design of Structures using Advanced Simulation Tools' [**9**], would be the first time that a similar section of floor would be dropped during one dedicated expeirmental campaign. This research allowed the characterization in the response to two extremes in loading, where the findings from the hard surface drop test is the subject of the first part of this two part paper.

This paper provides a complete section-by-section analysis of a simple box-beam structure typically found in metallic helicopters that was taken from the aft part of the main passenger section of a Westland WG30 helicopter developed in the late 1970s. This type of helicopter was chosen as being atypical of an all metallic design, which has been flight certified to crashworhtiness criteria defined through MIL-STD1210A and more recently, the aircraft survival design guidelines.

These regulations deal primarily with hard and soft soil surfaces and even in the latest incarnation, the joint service specification guide, there are still no provisions for ensuring a high level of survivability for an impact on water, or any certification tests related to impacts on water. The existing hard surface recommendations are completely inappropriate for an impact on water, as the main energy absorbing frames are effectively 'by-passed', because of the dominant behaviour of the skin.

The water drop test is described in two sections, with the first providing a description of the test facilities, the choice of boundary conditions and the instrumentation applied to the structure, and the second part will provide a detailed classification of the different failure modes observed. The aim of the current paper is to provide access to the detailed experimental observations and measurements taken by Cranfield University, which can be used to support future numerical methods validation. Having a detailed understanding of the collapse mechanism for this type of structure will be critical to understand fully the implications of this design on passenger safety and lead to the identification of potential design improvements for an improved crashworthy response.

2 SUBFLOOR SPECIMEN

The component floor was manufactured from an aluminium 2014 alloy and was taken from the aft part of the main passenger section of a WG30 helicopter, between STN1210A and 370A, as shown in Fig. 1. This component had a mass of 41 kg and was 2170 mm wide, 970 mm long, and 163 mm high. The dimensions of the main structural components can be found in Table 1.

The subfloor is a lattice construction consisting of longitudinal and lateral frames manufactured from metallic sheets. The longitudinal frames are reinforced by three evenly spaced L-section stiffeners and are attached to the upper seat track assemblies with a uniform rivet pitch of 25 mm. The lower parts are

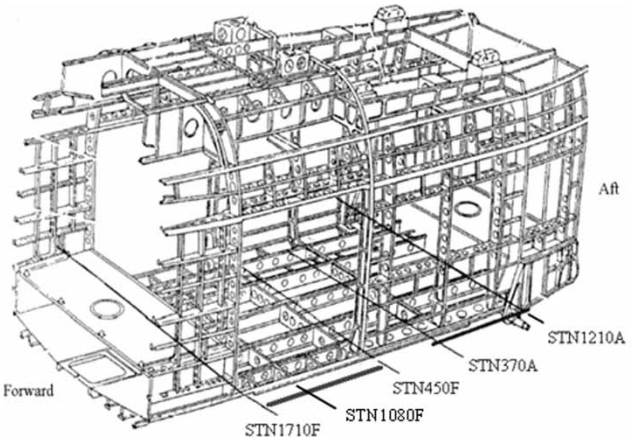

Fig. 1 Location of the component subfloor in relation to the main passenger section of the WG30

reinforced with z-section stiffeners, which also provide a riveted attachment to the lower skin.

The frames orientated in the transverse direction are also manufactured from metallic sheet and are typically shorter in length. STN370A consists of a combination of single and double skinned metallic frames, to which L-section brackets are riveted to provide attachment points for the passenger floor. These transverse frames are connected to the longitudinal frames via C-section overlaps to form individual box-sections. The transverse frames contain a central cut out for a longitudinal z-section stringer that provides structural rigidity for the skin.

The curved end-sections are riveted directly to the main longitudinal end frames, which provide a direct load path for the main engine and gearbox assemblies to the impacted surface. STN1210A represent an extremely strong construction, as the port and starboard landing gear attachments form part of this frame. The passenger section floor is attached via tapered screws and is manufactured from a composite material called Fibrelam, which consists of unidirectional glass fibres bonded to a honeycomb/aramid core. The outer skin is also manufactured from metallic sheets and riveted to all longitudinal and transverse frames.

Table 1 Dimensions of the principal components in the floor

Item	Length (mm)	Height (mm)	Thickness (mm)	Quantity (mm)	Material
V830	958.0	143.5	1.2	2	Al2024
V480	958.0	143.5	1.2	4	Al2024
V0	956.5	143.5	1.2	2	Al2024
STN370A	1655.0	144.5	1.2	1	Al2024
STN370A Reinforcement	361.0	143.0	0.7	2	Al2024
STN1210A	1660.0	174.0	1.5	1	Al2024
Z-stringer				9	
Web	953.5	31.0	0.9	–	Al2024
Lower flange	953.5	18.5	0.9	–	Al2024
Upper flange	953.5	10.5	0.9	–	Al2024
L-Stringers				13	Al2024
Web	20.0	140.0	0.9	–	Al2024
Flange	16.0	140.0	0.9	–	Al2024
Outer skin	1660.0	980.0	0.7	1	Al2024
Passenger floor	960.0	456.0	10.0	2	Fibrelam
	960.0	326.0	10.0	2	Fibrelam
	960.0	231.0	0.7	2	Al2024

3 WATER IMPACT FACILITY

The component floor was dropped at the water impact facility at CIRA in Italy (Centro Italiano Ricerche Aerospatziali), which consists of a 4 m deep tank and an 11 m high tower that guides the descent of the trolley to which the subfloor was rigidly attached [**15**]. This specialist test rig allowed the desired attitude of an 8 m/s near normal impact to be obtained, which allowed the collapse mechanisms to be identified through use of the following:

(a) global kinematics of the subfloor through accelerometers;
(b) pressure time histories on the skin via surface mounted transducers;
(c) high-speed video motion analysis (1000 frames per second for 1 s);
(d) posttest photographs of the resulting deformation;
(e) strain gauge data at various frame locations.

As can be seen in Fig. 2, the subfloor was attached to the guide trolley by means of 18 rods that fit directly into the seat rails. This was to ensure that the representative load paths of the seats and supporting structure were correctly passed into the structure. A breakdown of the ballast added to the trolley to take into account

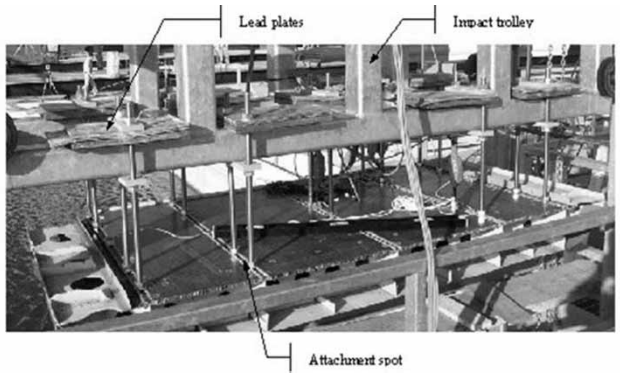

Fig. 2 Test rig designed by CIRA for the 8 m/s subfloor impact onto water, which shows the location of the ballast plates, together with the positions of the 18 seat rail attachment points [**10**]

Table 2 Distribution of mass for component subfloor

Item	Mass (kg)
Subfloor section	41.0
Impact trolley	338.4
Lead ballast	237.1
Mountings for subfloor	24.5
Extension cables	7.9
Total	648.9

the mass of the passengers, as well as the mass of the surrounding airframe, can be found in Table 2.

The test article was instrumented with accelerometers, pressure transducers, and strain gauges, sampling at 10 kHz. Before analogue to digital conversion, the signals were filtered through a low pass analogue filter in order to prevent any aliasing of the signal [**16**]. The experimental data was then filtered using a four-pole low-pass Butterworth filter, compliant to CFC1000.

The accelerometers were general-purpose EGE type sensors manufactured by Entran, used for both high output and high frequency sampling rates [**17**]. This company also supply EPL surface mounted stainless steel pressure sensors, which have a sealed pressure reference of 1 bar and are suitable for both static and dynamic measurements. In order to isolate the transducers from the deformation of the panels, the sensors were mounted on square steel plates that had a cross-section of 15 × 15 mm and a thickness of 2 mm. Biadhesive tape was then used to attach the sensors to the steel plate. All constituent parts of the data acquisition system were calibrated to SAE/J211 and also included two Kodak high-speed digital cameras.

4 POST-TEST ANALYSIS

The post-test report provided a basic overview of the response of the subfloor to this type of impact, but provided very little in the way of a detailed assessment of the different frame constructions, the degree of deformation, or the locations of material and rivet failure [**15**].

In order to characterize the main features of damage, the structure was divided into individual zones and a global coordinate system centred at the aft section of V0, which was positive in both the port and forward directions was defined. All measurements were taken relative to this coordinate system, which allowed the absolute relative deformation of the individual plastic hinges to be recorded, together with the heights of the compacted frames. In addition, the deflections of the skin were also measured.

For this analysis, only the port side will be analysed in detail, as the starboard side was found to be predamaged before the test. This was mentioned

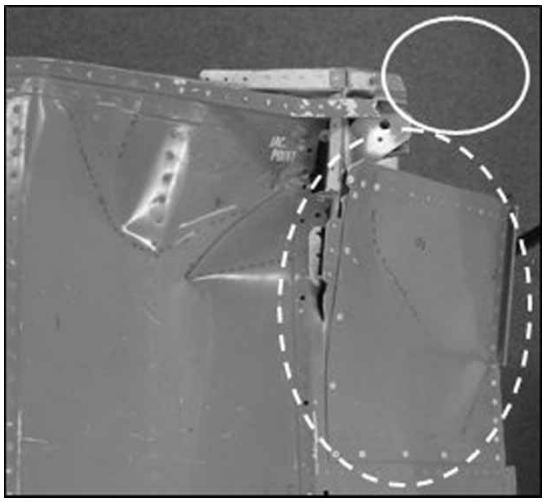

Fig. 3 Underside view of the starboard landing gear assembly that shows the location of the replaced skin panel (dashed circle) and the missing landing gear attachment (solid circle)

in the post-test report, as a replacement panel was riveted to this section as shown in Fig. 3, together with the removal of the port landing gear attachment. This changed the localized stiffness at this location, so damage to this side of the floor was neglected.

The aim of this analysis was to gain an understanding for the following:

(a) determine the global integrity of the under floor structure;
(b) assess the behaviour of the longitudinal and transverse frames;
(c) provide an assessment as to the effectiveness of the intersection joints;
(d) assess the behaviour of the skin and its role in energy absorption;
(e) identify the main locations of rivet and material failure;
(f) assess the deformation experienced by the skin.

5 MAIN FEATURES OF A WATER IMPACT

Figure 4 shows an overall view of the post-test article, where the instrumentation cables and passenger floor have been removed for clarity. As can be seen, the floor retains its global structural integrity, where the main features of damage and locations of material failure have been directly annotated onto this figure. One interesting feature concerns the different failure modes observed for the frame configurations used in its construction.

The main longitudinal frames, V830, V480, and V0, remain relatively undamaged, which is consistent with current understanding. The behaviour of the skin is

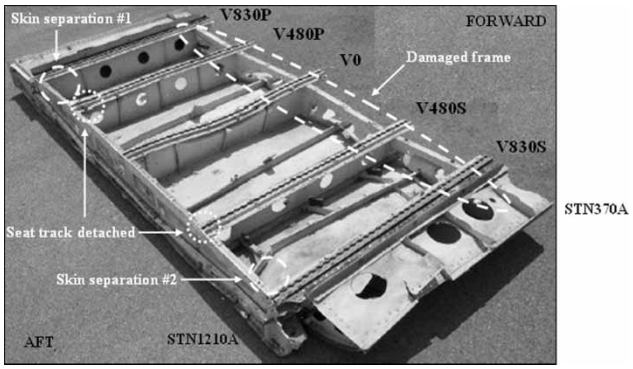

Fig. 4 Summary of the main locations of damage of the recovered subfloor

also consistent, as it deflects in-between these undamaged frames, with the peak occurring at the midpoints. This behaviour is clearly highlighted when one considers the pre- and post-test response of frame STN370A that forms the front part of this component in Fig. 5. This frame is subject to quite severe deformation due to the deflections of the skin, resulting in several locations of material failure.

The skin panels located between the longitudinal frames are subject to large deformations, as failure was observed in two limited areas between V480 and V830, which are highlighted as locations #1 and #2 in Fig. 4. However, the levels of damage are not symmetric, as it is more severe on the starboard side. The failure at location #2 can be discounted, as it is the consequence of the replaced panel. Despite this fact, this failure still serves as a severe example of the damage that could be potentially experienced by the surrounding components.

The location of skin failure on the port side (location #1) is the result of the surrounding structure being incredibly stiff in relation to the flexible skin. For example, the port landing gear attachment can be considered effectively rigid and its supporting effect on the surrounding structure results in the failure of the interconnecting rivets. This increase in skin deflection causes the propagation of material fractures along both lateral and longitudinal rivets lines, which in turn, permits further skin deflection and associated rivet failure.

Limited deformation is observed along the curved end sections, as the structure in this location is substantially reinforced by the landing gear assemblies on one side and by reinforcing brackets on the other. The skin deflections that occur are relatively minor, as the curvature of the skin redirects the water surface and minimizes the loading at these locations.

6 FRAME CONFIGURATIONS AND THEIR FAILURE MODES

The subfloor consists of a variety of different frame types, which will now be taken in turn and described in more detail. In order to provide a complete overview, consideration will be given to the transverse frames STN370A and 1210A first, followed by the longitudinal frames V0, V480, and V830.

6.1 STN370A

This frame is considered in two parts, as its construction varies along its length. Between V480 and V0, STN370A is single framed, whereas between V480 and V830, the construction changes to a double skinned configuration. This reinforcement has a profound effect on the failure modes observed.

Due to the inward deflection of the skin, the single frame buckles at the midpoint, as shown by the continuous and dotted lines in Fig. 6, which represent an inward and outward hinge, respectively. The upward movement of the skin causes the central z-stringer to cut into the frame, causing localized material failure in Fig. 7.

The double skinned frames between V830 and 480 do not fail in this way, as Fig. 8 demonstrates. This section of the floor is substantially reinforced by V830, coupled with the construction of the double skin, this means that very little deformation occurs in the vicinity of V830. Towards V480, severe frame deformation occurs due to the failure of the interconnecting rivets via tensile pull-out, resulting in a plastic hinge line that

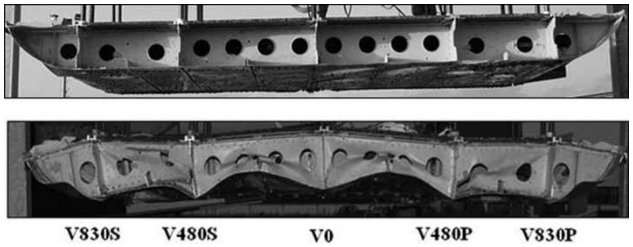

Fig. 5 Pre- and post-test response showing the degree of deformation along STN370A at the forward section of the subfloor

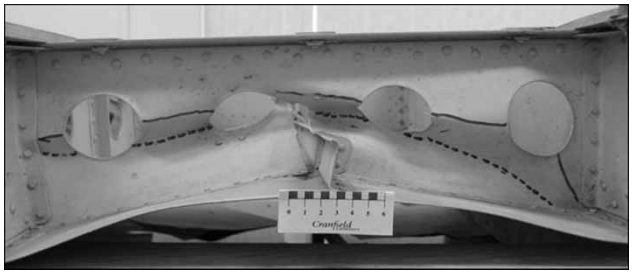

Fig. 6 The location of plastic collapse of STN370A located between V480S and V0

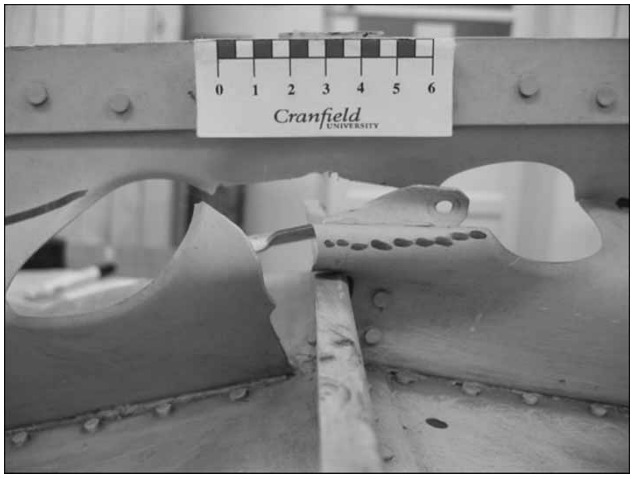

Fig. 7 Close up of the material failure that occurs along the single skinned section of STN370A, located between V0 and V480P, due to the upward deflection of the skin

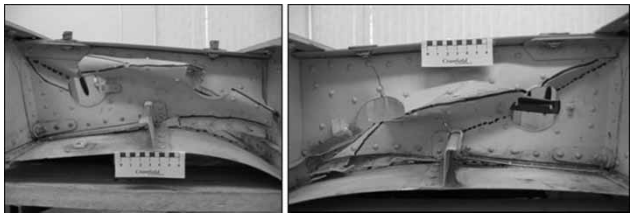

Fig. 8 The different failure modes observed for the double skinned frame of STN370A between V830 and V480 port (left) and starboard (right), due to the upward deflection of the skin

runs diagonally across this frame. The strong nature of this construction prevents the upward displacement of the central z-stringer, so no localized frame failure occurs.

6.2 STN1210A

STN1210A forms part of lower aft bulkhead and is a substantial component due to the attachment of the port and starboard landing gear assemblies, and the reinforcing rail that runs along its length, as shown in Fig. 9. As expected, no significant deformation is observed as this frame retains its structural integrity, with only slight damage observed at the base of the z-stringers, together with slight plastic hinge lines forming at the intersections with the longitudinal v-frames.

6.3 Longitudinal frames

The classification of longitudinal frame response has been categorized into three sections. The failure

Fig. 9 Due to the high strength construction of STN1210A, no deformation is observed

modes for the frames V0, V480, and V830 can be found in Figs 10(a) to (c), respectively.

1. Frame without holes (i.e. V0).
2. Frame with holes (i.e. V480P and S).
3. End frames with holes (i.e. V830P and S).

6.3.1 Configuration #1 – V0

The aft part of V0, situated between stations STN-1210A and 370A, consists of a single metallic sheet that is reinforced by three evenly spaced L-section stringers. The failure mode for this frame consists of single hinge line that forms in the upper part of this frame as shown in Fig. 10(a), which is a direct consequence of the proximity of the applied loading that was attached either side of the central stringer. The outward buckle results in the stringers adopting this failure mode, causing small localized material fractures at the peak of this deflection.

6.3.2 Configuration #2 – V480

This frame configuration can be found in Fig. 10(b) and is the most common, as it consists of a single metallic sheet reinforced with evenly spaced L-stringers and also contains four circular cut outs that act to reduce the weight of the frame. Limited deformation is observed, which is consistent with current understanding, as the current construction is not able to transfer the increase in water pressure to these energy absorbing components. Therefore, the available stroke is not utilized and very little energy is absorbed.

The deformation observed towards the aft part of this frame is caused by the failure of the upper seat track and STN1210A, due to the proximity of one of the pairs of attachment points located at the last two seat track positions shown in Fig. 11. This separation results in an upper hinge line that spreads to the midpoint of V480, as this frame now solely supports the loading. Also shown in Fig. 10(b) is the severity of the skin in relation to the height of the undamaged V480P,

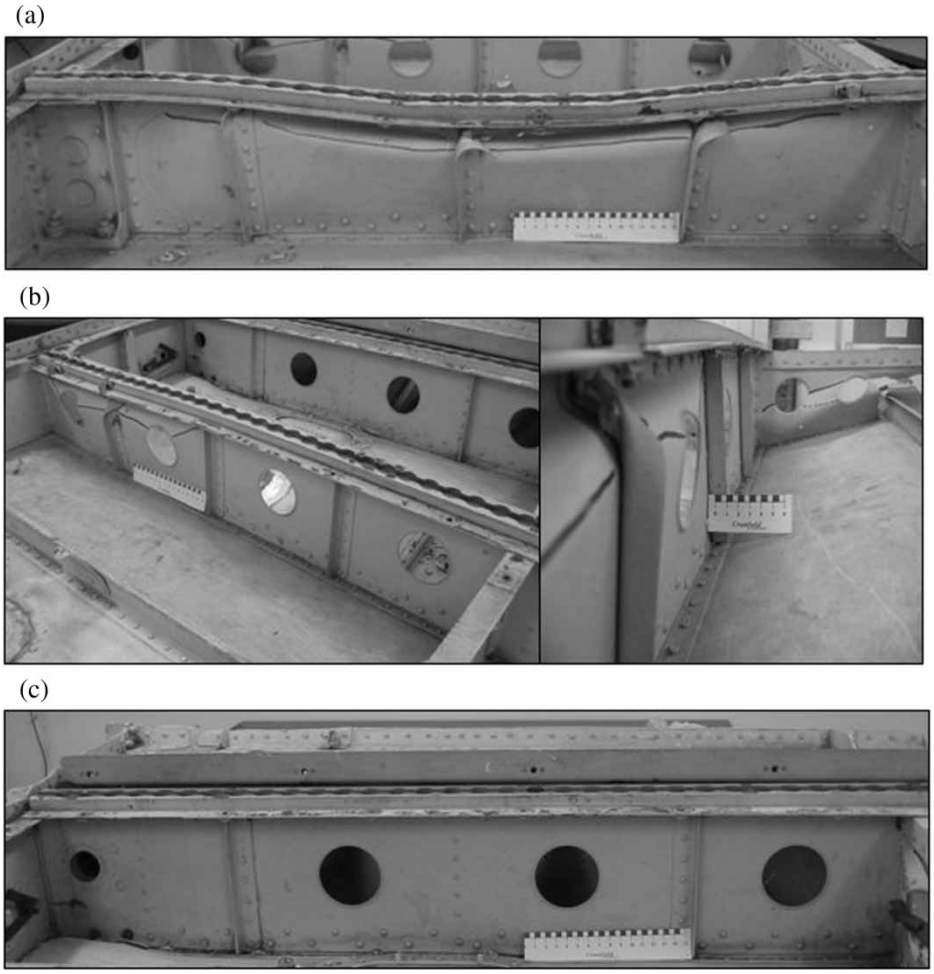

Fig. 10 Comparison between the different failure modes observed for (a) V0, (b) V480P, and (c) V830P. (The frame orientations are normal to the water surface)

which demonstrates quite succinctly the dominant behaviour of the skin for an impact on water.

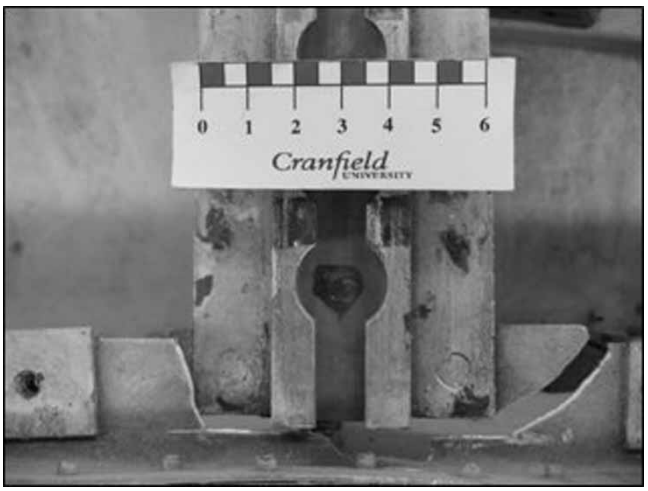

Fig. 11 Top down view of the shear failure of the upper seat track at the intersection between V480 and STN1210A

6.3.3 Configuration #3 – V830

The final frame configuration shown in Fig. 10(c) is similar in construction to configuration #2, except the frame does not have a vertical stringer located at the midpoint. Instead, this frame is directly riveted to a curved transverse end frame, which provides the vertical support. Due to the high strength nature of this construction in relation to the flexible skin, no deformation is observed.

To conclude, due to the high strength nature of the construction and the inability to transfer the membrane loads generated in the skin, the forces generated are insufficient to initiate collapse in the longitudinal frames. This lack of deformation means that their contribution to energy absorption will be small, as demonstrated by the comparison presented in Fig. 12 for the relative heights at different points along these frames. This infers that the failure strength of the structure is a critical parameter for a water impact and indicates that the current construction exhibits too high a failure strength, due to the inefficient use of structural collapse as an energy absorbing mechanism.

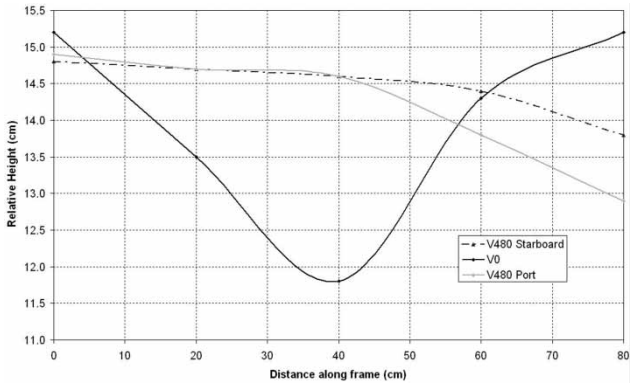

Fig. 12 Graph of compacted heights for the longitudinal frames which shows that the lack of collapse demonstrates that the membrane loads generated are insufficient to trigger collapse

7 INTERSECTION JOINTS

The collapse of a box section is heavily dependant upon the behaviour of the supporting frames, together with the collapse of the intersection joints. These joints are extremely strong, due to the plies that are riveted together and the reinforcing brackets that are used. As the loads encountered during a water impact are less than those that are generated during a hard surface impact, the membrane loads generated are insufficient to cause collapse as no deformation is observed [**18**]. The stabilizing effect of these joints will reinforce and support the frames, resulting in very little energy being absorbed, as shown in Fig. 13. Progressive collapse needs to be encouraged for the water impact case, if improvements in energy absorption are to be gained.

Fig. 13 A lack of intersection joint collapse is a common feature observed during a water impact, as the intersection between STN370A and V0 orientated normal to the water surface demonstrates

8 SKIN BEHAVIOUR AND ITS CONTRIBUTION TO ENERGY ABSORPTION

The membrane behaviour of the skin is of paramount importance for an impact on water, as the deflections form part of the energy absorbing process, due to the kinetic energy imparted to the water. An underside view of the skin response can be found in Fig. 14, which shows the port deformation in the region surrounding SNT370A.

In order to assess the deformation, deflection measurements were taken, which involved creating a measuring rig that used horizontal and vertical datums in order to determine the relative displacement of the skin from a fixed reference point. All measurements were taken relative to the intersection of V0 and STN1210A, due to the fact that no deformation occurs at this location. The skin was divided into nine zones and 51 measurements were taken at evenly spaced intervals, which include the deformation along STN370 and 1210A, together with measurements taken along the midpoint of the floor. Only port deflections were considered due to the starboard replacement panel that was added in Fig. 3.

The measurements can be found in Table 3 and are presented graphically in Fig. 15. A positive relative displacement means that the point is higher than the reference point (i.e. it has moved inside the internal structure of the subfloor), whereas a negative value indicates that the point is lower than the reference point.

As no frame collapse is observed for STN1210A, the displacement of the skin at these locations is

Fig. 14 Underside view of the port side taken after the drop test. Picture courtesy of CIRA [**10**]

Table 3 Comparison between the relative displacements of various points distributed across the skin, relative to a fixed reference point at the intersection of V0 and STN1210A

Location	X (±0.1cm)	Y (±0.1cm)	Relative Z displacement experiment (±0.1cm)
1	0.0	8.0	0.0
2	0.0	48.0	−0.3
3	0.0	87.0	−0.8
4	12.0	8.0	1.3
5	12.0	48.0	2.5
6	12.0	87.0	1.5
7	24.0	8.0	1.1
8	24.0	48.0	3.0
9	24.0	87.0	3.5
10	36.0	8.0	1.3
11	36.0	48.0	1.2
12	36.0	87.0	0.5
13	48.0	8.0	−0.5
14	48.0	48.0	−1.8
15	48.0	87.0	−2.4
16	56.5	8.0	0.5
17	56.5	48.0	0.8
18	56.5	87.0	−0.1
19	65.0	8.0	0.2
20	65.0	48.0	2.0
21	65.0	87.0	0.6
22	73.0	8.0	1.5
23	73.0	48.0	1.0
24	73.0	87.0	−0.1
25	80.0	8.0	1.1
26	80.0	48.0	0.0
27	80.0	87.0	−0.5

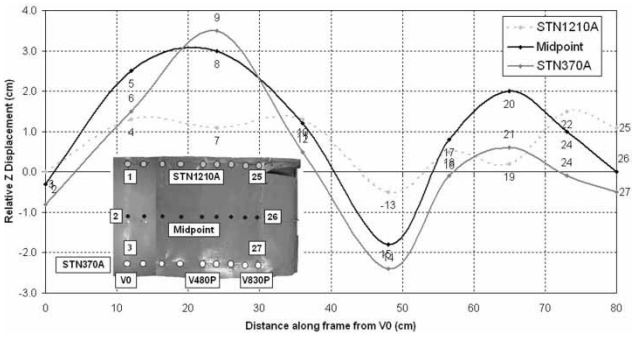

Fig. 15 Comparisons between the relative skin deflections near STN1210A, located between V0 and V830P. All measurements taken relative to aft of V0

small and is typically of the order of 1.5 cm. The skin deflections along the midspan and STN370A are comparable, which peaks at the midpoints in-between the longitudinal frames V0 and V480P. The deflections are of the order of 3 cm and correspond to the failure of the single skinned STN370A at this location, due to the interpenetration of the central z-stringer shown in Fig. 7.

Due to the distortion of STN370A, inward and outward deflections are also evident, which can be clearly seen in Fig. 5. The degree of skin deformation decreases in magnitude as one moves closer to V830P, due to the increase in strength of the construction and the lack of deformation observed. The midspan deflection is larger than STN370A when one compares locations 20 and 21. This difference is attributed to the fact that the increase in water pressure only has to overcome the structural rigidity provided by the reinforcing z-stringer, whereas frame collapse is required for STN370A.

Table 4 provides a comparison between the relative displacements for the skin at various port side locations for the curved end section, using the same reference point at the intersection of V0 and STN1210A. Due to the limited relative deformation presented in Fig. 16, the results demonstrate how the shape can cause the redirection of the water surface, which can be beneficial in minimizing the loading at these locations.

Table 4 Comparison between the relative displacements of various points distributed across the skin for the port end section, relative to aft of V0

Location	X (±0.1cm)	Y (±0.1cm)	Relative Z displacement experiment (±0.1cm)
28	−37.0	16.5	2.1
29	−37.0	0.0	15.2
30	−18.5	16.5	2.4
31	−18.5	0.0	15.2
32	0.0	16.5	2.8
33	0.0	0.0	15.5
34	10.0	16.5	3.0
35	10.0	0.0	15.5
36	20.0	16.5	3.3
37	20.0	0.0	15.6
38	30.0	16.5	3.5
39	30.0	0.0	15.6

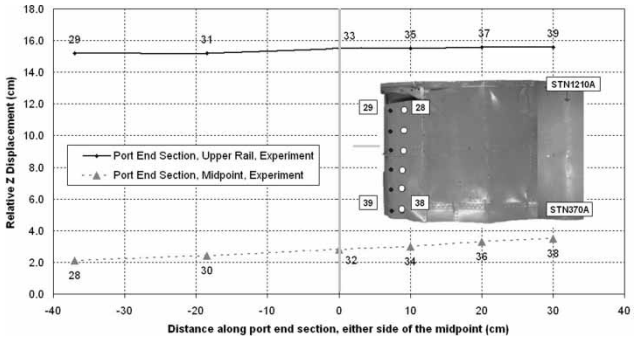

Fig. 16 Comparisons between relative skin deflections along lower and upper part of port curved end section. All measurements taken relative to the intersection of V0 and STN1210A

9 ACCELERATION TIME HISTORIES

After the drop test had been performed, it was found that the accelerations exceeded the range of the data acquisition system, as this was set to be sensitive to a maximum of 50 g. Therefore, no accurate data exists regarding the acceleration pulse shape, duration, or magnitude along any of the seat rails.

In order to provide an estimation for the whole body deceleration experienced by the guided trolley assembly, the displacement measurements shown in Fig. 17, were obtained from the two high-speed cameras located 20 and 5 m away from the drop tower, respectively. The images were calibrated against a fixed datum, where the velocity and acceleration time histories were obtained by discrete differentiation of the displacement data in Figs 18 and 19, respectively.

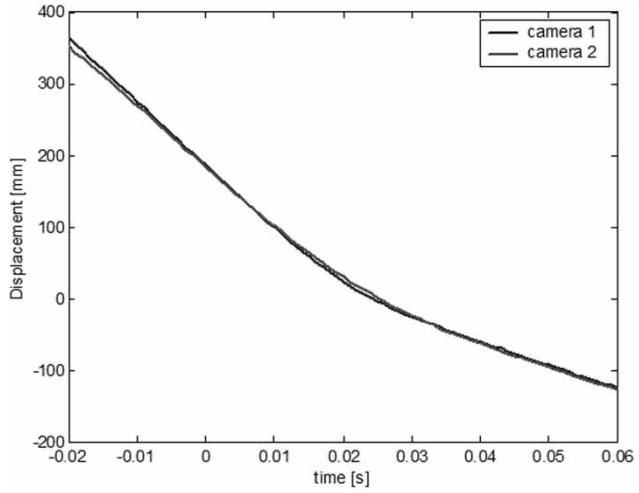

Fig. 17 The vertical displacement of the guided trolley assembly determined from the high-speed camera images

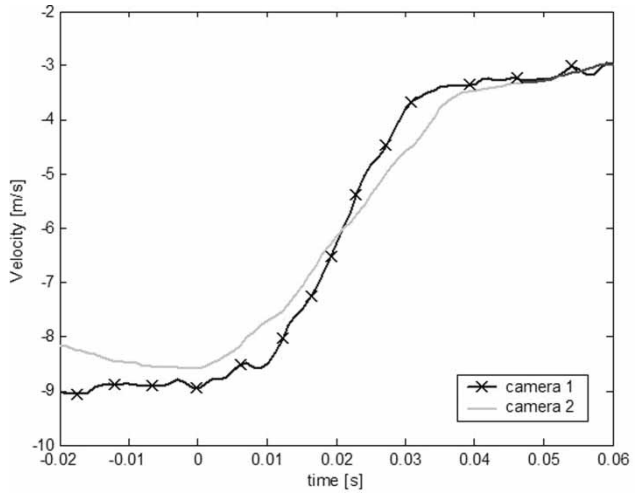

Fig. 18 The velocity time history of the trolley assembly was obtained by differentiating the displacement data obtained from the high-speed cameras

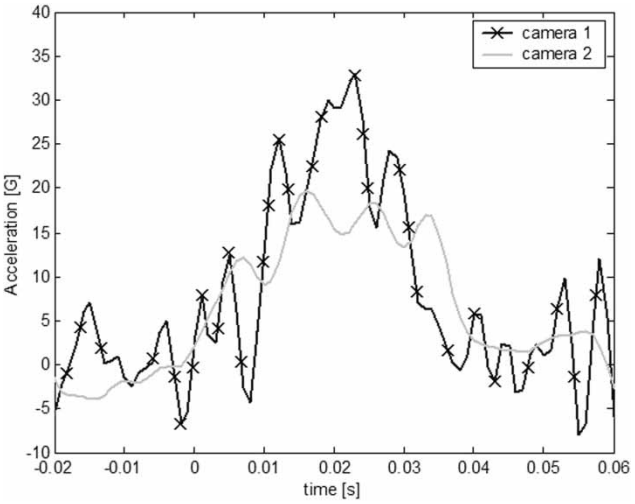

Fig. 19 The whole body deceleration of the trolley assembly was obtained by differentiating the velocities obtained from the high-speed camera displacement data

The velocity change of the trolley determined by the high-speed footage was supported by calculating the mean force pulse generated in the interval ($t_1 = 0$ ms, $t_2 = 30$ ms) from the pressure time histories and equating this to the change in momentum of the body. This change was estimated to be approximately 4 m/s, which provides confidence with the data determined from the high-speed cameras.

10 PRESSURE TIME HISTORIES

The pressure time histories can be an extremely difficult parameter to measure accurately due to cavitation effects that can cause severe oscillations in the pressure results, which is caused by a change in phase of the water, resulting in the formation and collapse of bubbles. This is an extremely complex phenomenon that can cause problems for experimentalists, due to the problems of repeatability between successive drop tests [**19**].

For example, Fig. 20 shows the results obtained for a pressure transducer located under the midpoint of V480P. As can be seen, the pressure rises to approximately 120 kPa, before going negative after 30 ms. The negative region is not an indication of cavitation, as it is an artificial effect caused by the inertial properties of the transducer. The oscillation of the sensor provokes this false reading, which can result in misinterpretation if the analyst is not aware of this effect. Removing this noise is difficult to achieve in practice and raises questions as to the validity of the results in this region.

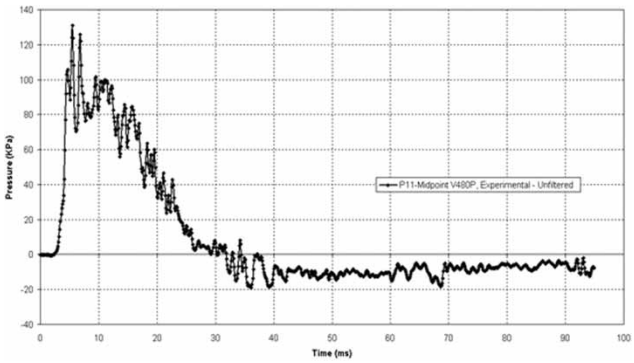

Fig. 20 Experimental pressure time history for P11 situated underneath the midpoint of V480P

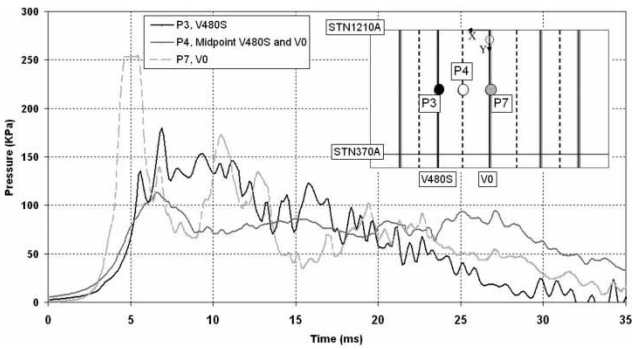

Fig. 21 Experimental pressure time histories for three different strength locations of the floor, namely V480S, V0 and the midpoint

The results presented in Fig. 21 provide a comparison between the pressure results obtained along the midpoint of V480P and V0, which represents 'hard' locations where little frame deformation occurs, together with the flexible skin section located in between these two frames where significant inward deflections occur and is termed a 'soft' location. The pressures recorded underneath the frames of P3 and P7, results in high pressures of approximately 179 and 253 kPa, respectively. The hard results are higher than those at the soft location, as a peak pressure of only 113 kPa is recorded. This is expected and can be explained by the differences in stiffness between the two locations, as the more deformable locations are better able to counteract the sudden increase in pressure due to yielding, resulting in the lower pressures being recorded.

11 CONCLUSIONS

The detailed frame-by-frame analysis presented in the current paper aims to provide an understanding of the response of a typical metallic under floor structure to an impact on water, by identifying its failure modes and providing quantitative data for the degree of skin deflection. The following is a summary of the main findings, which has led to the identification of design improvements that should be made to increase the water crashworthy characteristics of this design.

One of the main limitations concerns the non-crashworthy response of the current design, due to the inefficient use of the existing crumple potential of the under floor, as very little energy is absorbed by the frames of the intersection joints. This is caused by the lower loads that are encountered as the membrane loads generated are insufficient to trigger frame collapse, couple with the high failure strength of the existing construction.

The first recommendation concerns the very stiff sections of the subfloor that are too strong from a water impact point of view. This includes the intersection joints that form between the frames and the frames themselves. Consideration should be given to encourage frame collapse at lower loads through the use of geometry, material type, and the inclusion of triggers. The caveat with this approach is that if the failure strength is optimized for a water impact, a poor crashworthy response may occur during an impact onto a hard surface.

The second area for improvement concerns the development of the stiff intersection joints, as the collapse of a typical box-section is heavily dependant upon the failure of these joints. A proposed concept demonstrator solution to this problem can be found in reference [**18**]. This area of research is closely linked with the development of the skin, as successfully transferring the water pressure will be essential to encourage progressive collapse.

The dominant mechanism for energy absorption is through the ductile behaviour of the skin. Previous research has highlighted the benefit of using the infinite stroke that is available for an impact on water. However, maintaining skin integrity is essential in order to maintain the floatation capabilities of the helicopter, while at the same time, being able to generate sufficient membrane loads to cause collapse of the energy absorbing components within the design. This may be achieved through the use of specifically developed composite materials, such as tensor skins for example, which allow significant deflections without failing.

To conclude, it is proposed that a next generation design should encompass a passive dual role capability for hard and soft surface impacts, by being able to degrade the localized failure strength at key locations in the floor, depending upon the type of surface encountered. This would result in an optimized floor that has been specifically designed to fail at two different collapse loads; a higher failure strength for hard surface impacts through the use of composite crush cones for example, and a lower failure strength that

uses a combination of variable thickness frames and a deformable outer skin that has been specifically designed for an impact on water. This capability will significantly improve the crashworthy response of a metallic under floor structure and have a significant impact on improving passenger survivability during an impact on water.

ACKNOWLEDGEMENTS

This work was performed within the project CAST, which is an acronym for 'Crashworthiness of Helicopters on Water: Design of Structures using Advanced Simulation Tools', which is funded by the European Community under the 'Competitive and Sustainable Growth' programme (Contract G4RD-CT1999-0172).

The drop test was performed by Andrea Vigliotti at the Water Imact facility in CIRA, Italy.

REFERENCES

1 **von Karman, T.** The impact of seaplane floats during landing. NACA Technical Note 321, October 1929.

2 **Coltman, J. W.** and **Neri, L. M.** Analysis of US civil rotorcraft accidents for development of improved design criteria. National Specialists Meeting on Crashworthy Design of Rotorcraft, American Helicopter Society, 1986.

3 **Coltman, J. W., Domzalski, L.,** and **Arndt, S. M.** Evaluation of the crash environment for US navy helicopters … the hazards and navy response. National Specialists Meeting on Crashworthy Design of Rotorcraft, American Helicopter Society, Atlanta, Georgia, 1986.

4 **Chen, C. C. T., Muller, M.,** and **Fogary, K. M.** Rotorcraft ditchings and water related impacts that occurred from 1982 to 1989 – phase I. US Department of Transportation, FAA Technical Center, Atlantic City, October 1993, DOT/FAA/CT-92/13.

5 **Muller, M.** Rotorcraft ditchings and water related impacts that occurred from 1982 to 1989 – phase II. US Department of Transportation, FAA Technical Center, Atlantic City, October 1993, DOT/FAA/CT-92/14.

6 **Fasanella, E. L., Jackson, K. E.,** and **Lyle, K. H.** Finite element simulation of a full scale crash test of a composite helicopter. American Helicopter Society 56th Annual Forum, Virginia, USA, 2000.

7 **Wittlin, G., Smith, M., Sareen, A.,** and **Richards, M.** Airframe water impact analysis using a combined MSC/DYTRAN – DRI/KRASH approach. American Helicopter Society 53rd Annual Forum, Virginia Beach, Virginia, 29 April–1 May 1997.

8 **Wittlin, G., Schultz, M.,** and **Smith, M. R.** Rotary wing aircraft water impact test and analyses correlation. American Helicopter Society 56th Annual Forum, Virginia, USA, 2–4 May 2000.

9 **CAST.** Crashworthiness of helicopters onto water – design of structures using advanced simulation tools. Funded by the European Community under the 'Competitive and Sustainable Growth' programme (Contract G4RD-CT1999-0172), 2000–2003.

10 **CRAHVI.** Crashworthiness of aircraft for high velocity impact. Funded by the European Community under the 'Competitive and Sustainable Growth' Programme (Contract G4RD-CT-2000-00395), 2001–2004.

11 **Vicente, J. L. S., Beltran, F.,** and **Martinez, F.** Simulation of impact on composite fuselage structures. European Congress on Computational Methods in Applied Science and Engineering (ECOMAS), Barcelona, September 2000.

12 **McCarthy, M. A., Wiggenraad, J. F. M., Kohlgruber, D. F.,** and **Kamoulakos, D.** Finite element modelling of crash response of composite aerospace sub-floor structures. *Comput. Mech.*, 2000, **26**(3), 250–258.

13 **Ubels, L. C.** and **Wiggenraad, J. F. M.** Increasing the survivability of helicopter accidents over water. First European Survivability Workshop, Cologne-Wahn, Germany, 26–28 February 2002.

14 **Taher, S. T., Mahdi, E., Mokhtar, A. S., Magid, D. L., Ahmadun, F. R.,** and **Arora, P. R.** A new composite energy absorbing system for aircraft and helicopter. *Compos. Struct.*, 2006, **75**, 14–23.

15 **Vigliotti, A.** D3.2.5 – test report for sub structure no. 2. Task3.2/CIRA/3.2.5, Internal CAST report, May 2001.

16 **Vigliotti, A.** D3.3.2 instrument qualification report. Task3/CIRA/3.3.2, Internal CAST report, June 2001.

17 **Entran.** Available from http://www.entran.com/, accessed 18 January 2007.

18 **Vignjevic, R.** and **Meo, M.** A new concept for a helicopter sub floor structure, crashworthy in impacts on water and rigid surfaces. *Int. J. Crashworthiness*, 2002, **7**(3), 321–333.

19 **Anghileri, M.** D5.5.1 generic water impact tests. Task 5.5/PM/V5.5.1, Internal CAST report, 20th October 2001.